DOI: 10.13009/EUCASS2017-264

7^TH EUROPEAN CONFERENCE FOR AERONAUTICS AND AEROSPACE SCIENCES (EUCASS)

DOI: 264

Guidance, Navigation, and Control for Formation Flying Using Differential Drag

Shaked Chocron* *and Daniel Choukroun**†
Ben Gurion University of the Negev
Beer Sheva, 84105, Israel
chocros@post.bgu.ac.il · danielch@bgu.ac.il

Abstract

This work is concerned with the development of a scheme and algorithms for guidance, navigation and control, including attitude determination and control, for formation flying of small satellites via differential drag only along low Earth orbits. It includes 'real-life' features: a high variability air density, an attitude control algorithm for ballistic coefficient modulation, an attitude determination algorithm processing gyroscopes and typical vector measurements, and several relative navigation filters using relative position sensing and based on various air density design models. The realistic GNC/ADC scheme is tested under high integrity conditions. It enables closure of an initial distance of 70 km down to 2 km within eight orbits for two nanosatellites on low Earth orbits similar to the International Space Station. The degradation in the performances as compared to an ideal guidance scheme is due to the high variability of an unknown air density, the relative navigation errors, and the attitude control errors, in order of dominance. The best relative navigation filter appears to be a robust H_∞ filter. A comparison of that filter with the various Kalman filters shows a quicker convergence, a lesser sensitivity to the jumps in the air density, a similar steady-state accuracy, albeit with a noisier behavior.

1. Introduction

Spacecraft formation flight has been identified as a critical enabling technology for various scientific, commercial, and military space missions. Formation flight maintenance via differential aerodynamic drag has obvious advantages for nanosatellites with no or limited means of propulsion. Station keeping with differential drag is a proven concept and has been successfully demonstrated by OrbComm [1] for constellation station keeping of their satellites in supplement to propellant-based station keeping.

This paper investigates the guidance navigation and control performances of a couple of nanosatellites that exploit differential drag to achieve and maintain formation flight in low Earth orbits. The guidance algorithm introduced in [2, 3] guarantees convergence of relative motion to the origin in minimum time under limiting assumptions: predetermined differential drag modes, instantaneous switching among them, and perfect relative motion information. The first assumption relies on the perfect knowledge of the ballistic coefficients and of a constant air density. The second assumptions assumes an ideal mechanism for attitude or ballistic coefficient switching. The third assumption assumes a perfect navigation system. In this paper, all three assumptions are relaxed and a scheme for guidance, navigation and control is proposed and tested under 'realistic' conditions. Several 'real-life' features were added: a high variability air density, an attitude control algorithm that enables maneuvers to modify the ballistic coefficient, an attitude determination algorithm processing typical vector measurements available for small satellites, and several relative navigation filters based on various air density information modeling. The contribution of this paper are twofolds: A/ in the realm of relative navigation in the presence of high air density variability it introduces several filters based on various modeling assumptions on the air density and the relative motion equations: 1/ constant density perturbed by an additive white noise, 2/ constant density perturbed by a random walk, 3/ uncertain density of polytopic type, 4/ perfect information. Assumption 3 lends itself to a novel robust H_∞ relative navigation filter. B/ it introduces a feasible architecture, as shown in Fig. 1, for the GNC/ADC system for formation flight via differential drag onboard nonpropulsive small satellites and verifies the performances via realistic simulation conditions. The truth dynamics environment includes high-order gravity modeling for the orbit, drag and gravity-gradient torques as perturbations for the rotation, attitude control via reaction wheels and magnetorquers with continuous wheels desaturation, attitude determination via gyroscopes and typical line-of-sight measurements using state-of-art quaternion Kalman filtering.

DOI: 10.13009/EUCASS2017-264

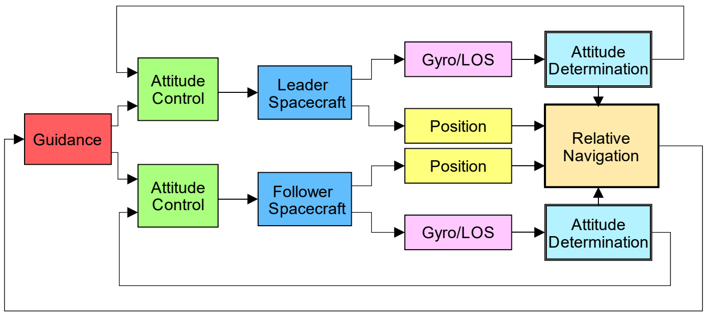

Figure 1: block diagram

Section 2 presents the relative navigation modeling and filters. Section 3 describes the attitude determination modeling and algorithm. Section 4 describes the attitude control modeling and algorithm. Section 5 presents the guidance scheme. Section 6 describes the satellites dynamics simulator. Section 7 shows the numerical results and Section 8 draws conclusions.

2. Relative Navigation

2.1 Preliminary results

Let $\mathbf{r} = (x, y, z)$ denote the position vector of the Follower S/C resolved along the frame $\mathcal{L}_L$. According to Ref. [4], the equations governing the dynamics of $\mathbf{r}$ can be approximated by a set of linear differential equations that account for the J_2 affect and a differential drag as follows:

$$\ddot{\boldsymbol{r}} + C\dot{\boldsymbol{r}} + K\boldsymbol{r} = \mathbf{d} \tag{1}$$

where, the forcing function $\mathbf{d}$, which stems from the differential drag, has the following expression:

$$\mathbf{d} = -\frac{1}{2}\left(\frac{1}{\beta_F} - \frac{1}{\beta_L}\right) r_{ref} n^2 \sigma_2 \begin{bmatrix} 0 \\ 1 \\ 0 \end{bmatrix}, \tag{2}$$

the damping matrix C and the stiffness matrix K are expressed as follows:

$$C = n \begin{bmatrix} \frac{1}{2}\frac{1}{\beta_F}\sigma_1 & -2c & 0 \\ 2c & \frac{1}{\beta_F}\sigma_1 & 0 \\ 0 & 0 & \frac{1}{2}\frac{1}{\beta_F}\sigma_1 \end{bmatrix} \tag{3}$$

$$K = n^2 \begin{bmatrix} -\left(5c^2 - 2\right) & -\frac{1}{2}\left(\frac{1}{\beta_F} + \frac{3}{\beta_L}\right)\sigma_2^2 & 0 \\ \frac{1}{2}\left(\frac{2}{\beta_F} - \frac{3}{\beta_L}\right)\sigma_2^2 & 0 & 0 \\ 0 & 0 & \left(3c^2 - 2\right) \end{bmatrix}, \tag{4}$$

and σ_1, σ_2 and β are defined as follows:

$$\sigma_1 = 1 - \frac{\omega_e}{n}\cos i_{ref}\,, \quad \sigma_2 = 1 - 2\frac{\omega_e}{n}\cos i_{ref}\,, \quad \beta = \left(\rho\frac{C_D S}{m} r_{ref}\right)^{-1} \tag{5}$$

In Eqs. (1) to (5), the time-invariant parameters n, r_{ref}, i_{ref} denote the mean orbital rate, the radius, and the inclination, respectively, of a reference circular orbit; c denotes a J_2 dependent coefficient, ω_e denotes the Earth rotation rate, C_D denotes the satellite drag coefficient, m denotes the satellite mass, S denotes a satellite cross-sectional area of reference, and ρ denotes the atmosphere's density along the reference orbit. The coefficients $\frac{1}{\beta_L}$ and $\frac{1}{\beta_F}$ are non-dimensional ballistic coefficients of the Leader and Follower.

DOI: 10.13009/EUCASS2017-264

2.2 Design Model in State-space

Let $\mathbf{x}$ denote the state vector defined as follows:

$$\mathbf{x} = (x, y, \dot{x}, \dot{y}, z, \dot{z}) \tag{6}$$

Noting that the dynamics of $\mathbf{x}$ can be controlled via the term $\left(\frac{1}{\beta_L} - \frac{1}{\beta_F}\right)$, and rewriting Eq. (1) yields the following process equation for $\mathbf{x}$ in state-space form:

$$\dot{\mathbf{x}} = A\,\mathbf{x} + Bu \tag{7}$$

where

$$A = \begin{bmatrix} \cdot & \cdot & 1 & \cdot & \cdot & \cdot \\ \cdot & \cdot & \cdot & 1 & \cdot & \cdot \\ n^2\left(5c^2-2\right) & \frac{n^2}{2}\left(\frac{1}{\beta_F}+\frac{3}{\beta_L}\right)\sigma_2^2 & -\frac{n}{2}\frac{1}{\beta_F}\sigma_1 & 2nc & \cdot & \cdot \\ -\frac{n^2}{2}\left(\frac{2}{\beta_F}-\frac{3}{\beta_L}\right)\sigma_2^2 & \cdot & -2nc & -\frac{n}{\beta_F}\sigma_1 & \cdot & \cdot \\ \cdot & \cdot & \cdot & \cdot & \cdot & 1 \\ \cdot & \cdot & \cdot & \cdot & n^2\left(3c^2-2\right) & -\frac{n}{2}\frac{1}{\beta_F}\sigma_1 \end{bmatrix} \tag{8}$$

$$B = \begin{bmatrix} \cdot & \cdot & \cdot & \frac{n^2}{2}\sigma_2 r_{ref}^2\rho & \cdot & \cdot \end{bmatrix}^T \tag{9}$$

$$u = \left.\frac{C_D S}{m}\right|_L - \left.\frac{C_D S}{m}\right|_F \tag{10}$$

and $\cdot$ denotes zeros in all above expressions. This process model emphasizes two features: 1/ the control variable u depends primarily on the satellites' cross-sectional reference areas and therefore on the satellites' attitudes, 2/ the input matrix B is a function of the atmospheric density, which is typically difficult to know exactly. Notice that the dynamics matrix A depends on ρ as well but to a lesser extent, by several orders of magnitude, than the matrix B. The impact of the air density uncertainty on the A matrix will be neglected. A measurement of the relative position is assumed to be acquired by the satellites, i.e.

$$\mathbf{z}_N = H_N\,\mathbf{x} + \mathbf{v}_N \tag{11}$$

where

$$H_N = \begin{bmatrix} 1 & \cdot & \cdot & \cdot & \cdot & \cdot \\ \cdot & 1 & \cdot & \cdot & \cdot & \cdot \\ \cdot & \cdot & \cdot & \cdot & 1 & \cdot \end{bmatrix} \tag{12}$$

and the measurement error is assumed to be an additive zero-mean white noise with known covariance $R_N = \sigma_N^2 I_3$.

2.3 Atmospheric density models and relative navigation algorithms

The Truth model for the atmospheric density is assumed to be the 2001 United States Naval Research Laboratory Mass Spectrometer and Incoherent Scatter Radar Exosphere (NRLMSISE-00 Atmosphere Model [5]). Yet the associated computation load, along with the unavoidable large uncertainty in ρ, might justify simplifying assumptions about the variability of ρ while yielding still satisfactory navigation performances. In the following, various Design models are proposed for ρ and the relative motion dynamics and, thus, various relative navigation algorithms are developed.

2.3.1 Model 0: Known air density

The air density, as evaluated from the NRLMSISE-00 Atmosphere Model, is assumed to be exactly known and is treated as a deterministic parameter in the design model for relative navigation. In this work we assume: $\rho_0 = 5 \cdot 10^{-10}\left[kg\,m^{-3}\right]$, a typical value at 400 km height.

2.3.2 Model 1: White noise

The air density model assumes that ρ is a random process with a constant and known expected value, ρ_0, and a zero-mean white noise process for the deviations from it at any time t.

$$\rho(t) = \rho_0 + w(t) \quad w \sim \mathcal{WN}(0, \sigma_{\rho 1}^2) \tag{13}$$

DOI: 10.13009/EUCASS2017-264

Using Eq. (13) in the state-space process equation (7) yields

$$\dot{\mathbf{x}} = A\,\mathbf{x} + B(\rho_0)u + Gw \tag{14}$$

where

$$G = \begin{bmatrix} \cdot & \cdot & \cdot & \frac{n^2}{2}\sigma_2 r_{ref}^2\, u & \cdot & \cdot \end{bmatrix}^T \tag{15}$$

Assuming that the external input u is a known deterministic variable, Eqs. (14),(11), describes a valid state-space system, for which a Kalman filter can be developed in order to estimate the state vector $\mathbf{x}$ of the relative position and velocity of the Follower with respect to the Leader. The Kalman filter equations are well-known and need not be written here. More details on the implementation will be provided in the section dedicated to the numerical results.

2.3.3 Model 2: Random Walk

The assumption on the air density is similar to Model 1 except that the deviation is here modeled as a Random Walk with intensity $\sigma_{\rho 2}$, i.e.

$$\rho(t) = \rho_0 + \eta(t) \tag{16}$$

$$\dot{\eta} = w(t) \quad w \sim \mathcal{WN}(0, \sigma_{\rho 2}^2) \tag{17}$$

The standard technique of state-augmentation yields the augmented state:

$$\mathbf{y} = (\,\mathbf{x}, \eta) \tag{18}$$

which process model is derived from Eq. (7) by appending to the matrix A in Eq. (8) a row of zeros and the column G as given in Eq. (15). The proposed algorithm is a Kalman filter that will estimate the augmented state.

2.3.4 Model 3: Input Disturbance and Parameter Uncertainty

The approach consists in considering the differential drag forcing term in Eq. (7) as a finite-energy disturbance and the density as a parameter with polytopic uncertainty. The rational for this approach is that the differential drag acceleration incorporates variables on which our knowledge is limited or noisy, like the drag coefficient or the satellites' orientations. A precise evaluation of the differential drag might thus prove elusive. Instead one may follow the path of estimating the relative motion in presence of the worst-case differential drag. Further, while the variability of the air density makes tracking difficult, knowing its bounds is easier. The upper and lower bounds are considered as vertices in the parameter space and a robust $\mathcal{H}_\infty$ filter is developed. Let α be defined as follows:

$$\alpha = \frac{n^2}{2}\sigma_2 r_{ref}^2\,\rho \tag{19}$$

A simple analysis suggests the following values of the vertices:

$$\alpha(1) = -10^{-3} \quad \alpha(2) = 10^{-3} \tag{20}$$

yielding two vertices $B(1)$ and $B(2)$ for the system matrix $B(\rho)$ in Eq. (7). The robust $\mathcal{H}_\infty$ filter equations are written below for the steady-state case.

$$\dot{x}_c = A_c x_c + B_c y \tag{21}$$

$$\hat{x} = C_c x_c + D_c y \tag{22}$$

the LMI system given as

$$\begin{bmatrix} A^T X + XA + B_F C_2 + C_2^T B_F & XA + A_F + B_F C_2 + A^T R & XB_1^{(i)} + B_F D_{21} & C_1^T - C_2^T D_F^T \\ * & A^T R + RA & RB_1^{(i)} & C_1^T - (D_F C_2 + C_F)^T \\ * & * & -\gamma^2 I & -D_{21} D_F^T \\ * & * & * & -I \end{bmatrix} < 0 \tag{23}$$

$$\begin{bmatrix} X & R \\ * & R \end{bmatrix} > 0, \quad \gamma \rightarrow \text{minimum} \tag{24}$$

where

$$A_F \triangleq MA_cR, \;\; B_F \triangleq MB_c, \;\; C_F \triangleq C_cR, \;\; M \triangleq I - XR^{-1} \tag{25}$$

The result of the LMI solution described above yields the filter matrices A_c, B_c , C_c and D_c for the filter.

DOI: 10.13009/EUCASS2017-264

3. Attitude Determination

The two satellites are assumed to be equipped with identical attitude sensing suites and attitude determination algorithms. The subscripts L and F will thus be omitted for the sake of simplicity.

3.1 Sensors mathematical model

3.1.1 Rate gyroscope

The attitude sensing system comprises a three-axis strapdown rate gyroscope that provides angular velocity measurements of the body frame $\mathcal{B}$ with respect to the inertial frame $\mathcal{I}$, resolved along $\mathcal{B}$. A widely used model [6] assumes that the gyro output is corrupted by a drift and a white noise and that the drift is modeled as a random walk. Other errors, such as misalignment angles and scale factors are discarded but can easily be incorporated to the model via state augmentation. Equations (26),(27) summarize the proposed gyro model:

$$\tilde{\omega} = \omega + \boldsymbol{\mu} + \boldsymbol{\eta}_v \tag{26}$$

$$\dot{\boldsymbol{\mu}} = \boldsymbol{\eta}_u \tag{27}$$

where $\tilde{\omega}$ denotes the gyro measurement, $\boldsymbol{\mu}$ denotes the drift and $\boldsymbol{\eta}_v$, $\boldsymbol{\eta}_u$ denote zero-mean white noise vectors with covariance matrices $\sigma_v^2 I_3$ and $\sigma_u^2 I_3$, respectively.

3.1.2 Vector measurements

The attitude sensing system also features devices that provide vector measurements. The current study assumes that two vector measurements are simultaneously acquired at each sampling time. The inertial projections of these vectors are assumed to be time-invariant during the time laps of interest, i.e. several periods of revolution around Earth. This is typical of line-of-sights to stars or to the Sun. Let $\mathbf{s}$ denote the projection of a measured vector along $\mathcal{I}$ and let $\mathbf{b}$ denote the associated noisy vector measurement, then the measurement model is described as follows:

$$\mathbf{b} = D(\mathbf{q})\mathbf{s} + \boldsymbol{\delta b} \tag{28}$$

where $\mathbf{q}$ denotes the quaternion from $\mathcal{I}$ to $\mathcal{B}$, $D(\mathbf{q})$ denotes the attitude matrix associated with $\mathbf{q}$, and $\boldsymbol{\delta b}$ denotes the measurement noise vector, modeled as a zero-mean white Gaussian noise with covariance matrix $\sigma_b^2 I_3$.

3.2 Attitude estimation algorithm

This work implements the widely used quaternion Multiplicative Extended Kalman Filter (MEKF) [7], where the gyro measurements are used for kinematics propagation and the vector measurements are processed in order to update the gyro drift and to estimate the quaternion. The estimated states are thus the attitude quaternion from $\mathcal{I}$ to $\mathcal{B}$ and the gyro drift, i.e. seven states. The linearized perturbations model however features the Euler vector of the estimation error rotation, denoted by $\boldsymbol{\theta}$, rather than the algebraic quaternion estimation error, and is thus of dimension six, rather than seven. Since the MEKF development differs from the standard Kalman filter, and for the sake of completeness, the MEKF equations are summarized as follows:
Initialization: $\widehat{\mathbf{q}}(0), \widehat{\boldsymbol{\mu}}(0), P_A(0)$, where $P_A(0)$ denotes the 6×6 initial estimation error covariance matrix.
Time propagation: Given $\widehat{\mathbf{q}}_{k/k}, \widehat{\boldsymbol{\mu}}_{k/k}, P_A(k/k)$

$$\widehat{\boldsymbol{\omega}}_{k/k} = \tilde{\omega} - \widehat{\boldsymbol{\mu}}_{k/k} \tag{29}$$

$$\frac{d}{dt}\widehat{\mathbf{q}}(t/t_k) = \frac{1}{2}\begin{bmatrix} -\left[\widehat{\boldsymbol{\omega}}_{k/k}\times\right] & \widehat{\boldsymbol{\omega}}_{k/k} \\ -\widehat{\boldsymbol{\omega}}_{k/k} & 0 \end{bmatrix}\widehat{\mathbf{q}}(t/t_k) \tag{30}$$

$$\frac{d}{dt}\widehat{\boldsymbol{\mu}}(t/t_k) = \mathbf{0} \tag{31}$$

$$F_A = \begin{bmatrix} -\left[\widehat{\boldsymbol{\omega}}_{k/k}\times\right] & I_3 \\ \cdot & \cdot \end{bmatrix} \tag{32}$$

$$Q_A = \begin{bmatrix} \sigma_v^2 I_3 & \cdot \\ \cdot & \sigma_u^2 I_3 \end{bmatrix} \tag{33}$$

$$\frac{d}{dt}P_A = F_A P_A + P_A F_A^T + Q_A \tag{34}$$

DOI: 10.13009/EUCASS2017-264

Measurement update: Given $\widehat{\mathbf{q}}_{k+1/k}, \widehat{\boldsymbol{\mu}}_{k+1/k}, P_A(k+1/k)$

$$\widehat{\mathbf{b}}_{k+1/k} = A(\widehat{\mathbf{q}}_{k+1/k})\mathbf{s}_{k+1} \tag{35}$$

$$H_A = \begin{bmatrix} -[\widehat{\mathbf{b}}_{k+1/k}\times] & \cdot \end{bmatrix} \tag{36}$$

$$R_A = \sigma_b^2 I_3 \tag{37}$$

$$S_{k+1} = H_A P_A H_A^T + R_A \tag{38}$$

$$K_{k+1} = P_A(k+1/k) H_A^T S_{k+1}^{-1} \tag{39}$$

$$P_A(k+1/k+1) = (I_6 - K_{k+1}H_A)P_A(k+1/k)(I_6 - K_{k+1}H_A)^T + K_{k+1}R_A K_{k+1}^T \tag{40}$$

$$\begin{pmatrix} \widehat{\boldsymbol{\theta}} \\ \widehat{\boldsymbol{\mu}} \end{pmatrix}_{k+1/k+1} = \begin{pmatrix} \cdot \\ \widehat{\boldsymbol{\mu}}_{k+1/k} \end{pmatrix} + K_{k+1}(\mathbf{b}_{k+1} - \widehat{\mathbf{b}}_{k+1/k}) \tag{41}$$

$$\delta\widehat{\mathbf{q}} = \begin{pmatrix} \frac{1}{2}\,\widehat{\boldsymbol{\theta}} \\ 1 \end{pmatrix} \frac{1}{\sqrt{1 + \|\,\widehat{\boldsymbol{\theta}}\|^2}} \tag{42}$$

$$\widehat{\mathbf{q}}_{k+1/k+1} = \widehat{\mathbf{q}}_{k+1/k} \otimes \delta\widehat{\mathbf{q}} \tag{43}$$

The measurement update is described for any vector measurement and is sequentially repeated if several vector observations are acquired. Equation (42) performs a brute-force normalization of the estimation error quaternion. Equation (43) describes the quaternion multiplication between the a priori estimate $\widehat{\mathbf{q}}_{k+1/k}$ and the estimation error $\delta\widehat{\mathbf{q}}$. It is a sequence of two rotation bringing first the $\mathcal{I}$ frame to the a priori estimated $\mathcal{B}$ frame and then to the a posteriori estimated $\mathcal{B}$ frame. The algorithms are identical on-board the Leader and the Follower, yielding the following estimates: $(\widehat{\omega}_L, \widehat{\mathbf{q}}_{\mathcal{L}}^{\mathcal{I}}, \widehat{\omega}_F, \widehat{\mathbf{q}}_{\mathcal{F}}^{\mathcal{I}})$. These outputs have two purposes: 1/ to calculate the ballistic coefficients and, thus, the differential drag acting on the relative motion, and 2/to calculate the tracking errors that drive the Attitude control algorithm.

4. Attitude Control

This section provides an overview of the Attitude Control system and algorithm. It is adapted from Ref. [8].

4.1 Quaternion Feedback Regulator

The quaternion feedback control law implemented here was introduced in [9], and is used to calculate a control torque which will rotate the satellite to the desired attitude. The following control law is given to calculate the required control torque

$$\mathbf{T}_r = -dJ\boldsymbol{\omega}_e - kJ\mathbf{q}_e \tag{44}$$

where J is the satellite tensor of inertia expressed in $\mathcal{B}$, d and k are scalar gain parameters, $\boldsymbol{\omega}_e$ is the error between the estimated inertial rotational rate vector and the desired one, expressed in the body frame, and $\mathbf{q}_e$ is the vector part of the quaternion that describes the rotation from the desired body frame to the estimated body frame. Let $\mathbf{q}_d$ denote the quaternion from the inertial frame to the desired frame, then

$$\mathbf{q}_e = \Xi_d^T \widehat{\mathbf{q}} \tag{45}$$

where

$$\Xi_d^T = \begin{bmatrix} q_{d_4} & q_{d_3} & -q_{d_2} & -q_{d_1} \\ -q_{d_3} & q_{d_4} & q_{d_1} & -q_{d_2} \\ q_{d_2} & -q_{d_1} & q_{d_4} & -q_{d_3} \end{bmatrix} \tag{46}$$

and $q_{d_i} = \mathbf{q}_d(i)$ for $i = 1, 2, 3, 4$. Let ω_d denote the angular rate of the desired frame with respect to the inertial frame, then

$$\omega_d = 2\,\Xi_d^T \dot{\mathbf{q}}_d \tag{47}$$

where $\dot{\mathbf{q}}_d$ and thus $\dot{\mathbf{q}}_d$ are a direct result of the desired mode of operation provided by the Guidance system. Notice that ω_d, as computed in Eq. (47), is expressed along the axes of the desired frame. The error vector, $\boldsymbol{\omega}_e$, is computed as follows:

$$\omega_e = D_{\mathcal{B}}^{\mathcal{D}}\,\omega_d - \widehat{\omega} \tag{48}$$

DOI: 10.13009/EUCASS2017-264

where $D_{\mathcal{B}}^{\mathcal{D}}$ is the transformation matrix from the desired frame to the body frame, such that ω_e is expressed in the body frame. The above proportional-derivative control law was successfully implemented on numerous satellites (see e.g. [10]). In the full actuation and perturbation free case, it is shown in [11] that the closed-loop controlled system is globally asymptotically stable.

4.2 Torque allocation and actuation

Each satellite is equipped with three reaction wheels and three magnetic torquers. One possibility is to let the reaction wheels deliver the entire required torque, $\mathbf{T}_r$, and let them be unloaded by the magnetorquers, when needed. However, this approach is likely to rapidly lead the reaction wheels to saturation. In order to ease on the reaction wheels the magnetorquers also are used and deliver part of the torque $\mathbf{T}_r$, unless unloading is needed, which receives higher priority than the control effort. Control torque allocation to the magnetorquers and the wheels is achieved following a geometric approach [12]. In compliance with the physical limitation of magnetic torquing, the torque allocated to the magnetorquers, denoted by $\mathbf{T}_{mtq_c}$, consists of the projection of the required torque on the plane orthogonal to the magnetic field vector $\mathbf{B}$. Given $\mathbf{B}$ and $\mathbf{T}_r$, the required magnetic dipole, $\mathbf{m}_c$, is computed as follows:

$$\mathbf{m}_c = \frac{\mathbf{B} \times \mathbf{T}_r}{||\mathbf{B}||^2} \tag{49}$$

It can then be easily shown that the magnetic torque $\mathbf{T}_{mtq_c}$ is expressed as follows:

$$\mathbf{T}_{mtq_c} = \mathbf{m}_c \times \mathbf{B} = \left(I_3 - \frac{\mathbf{B}\mathbf{B}^T}{||\mathbf{B}||^2} \right) \mathbf{T}_r \tag{50}$$

which is the sought orthogonal projection. The reaction wheels are actuated such as to deliver the remainder of the required torque. Thus, given $\mathbf{B}$ and $\mathbf{T}_r$, the commanded angular momentum rate in the wheels is computed as follows:

$$\dot{\mathbf{h}}_c = -\frac{\mathbf{B}\mathbf{B}^T}{||\mathbf{B}||^2} \mathbf{T}_r \tag{51}$$

Hence, the torque applied by the wheels on the spacecraft is

$$\mathbf{T}_{rw_c} = -\dot{\mathbf{h}}_c = \frac{\mathbf{B}\mathbf{B}^T}{||\mathbf{B}||^2} \mathbf{T}_r \tag{52}$$

which shows that the total control torque applied by the magnetorquers and the reaction wheels, $\mathbf{T}_c = \mathbf{T}_{mtq_c} + \mathbf{T}_{rw_c}$ is indeed equal to the required torque $\mathbf{T}_r$. To summarize, given $\mathbf{T}_r$ from Eq. (44), and $\mathbf{B}$ from magnetometers, the magnetorquers' magnetic dipole vector is commanded via Eq. (49) and the reaction wheels are commanded via Eq. (51). This allocation scheme is used in all modes when reaction wheels are far from saturation. The load dividing scheme delays the saturation of the reaction wheels since part of the required torque is delivered by the magnetorquers, but its design does not address this issue specifically. The desaturation issue is addressed in the implemented attitude control scheme following the Novel Unloading method presented in Ref. [8].

5. Guidance

The implemented guidance scheme yields a differential drag switching strategy, following the approach introduced in Ref. [3], which is described here for the sake of completeness.

Formation flight equations

It is well known, using for instance Clohessy-Wiltshire equations [13], that the satellites relative motion is a 2x1 ellipse whose center is constant in the radial direction but drifts in the along-track direction. It can be further shown that the average relative position of the follower, or alternatively the center of the 2x1 ellipse, can be expressed as

$$\bar{x} = \frac{2c^2}{2-c^2} x + \frac{2c}{(2-c^2)\,n} \dot{y}$$

$$\bar{y} = y - \frac{2c}{(2-c^2)\,n} \dot{x}$$

DOI: 10.13009/EUCASS2017-264

An algorithm was introduced in Ref. [3] that controls the position and size of the relative motion ellipse via a switching strategy of the differential drag. Two motion variables, α and β, are defined as the difference between the actual and mean position variables along the radial and in-track directions, $\alpha = x - \bar{x}$ and $\beta = y - \bar{y}$. This transformation leads to two uncoupled, second order linear differential equations:

$$\ddot{\bar{y}} = \frac{2 - 5c^2}{2 - c^2} a_y \tag{53}$$

$$\ddot{\beta} + \left(2 - c^2\right) n^2 \beta = \frac{4c^2}{2 - c^2} a_y \tag{54}$$

where a_y denotes the differential drag acceleration. Controlling $\bar{y}$, whose dynamics are a double integrator, will simultaneously control $\bar{x}$, and controlling β, whose dynamics are a harmonic oscillator, will simultaneously control α.

Maneuvering strategy

The parabolic control trajectories for the double integrator of Eq. (53) in the $x_1 = \bar{y}$, $x_2 = \dot{\bar{y}}$ plane are plotted in Fig. 2. The optimal time control solution to the origin involves a maximum of two switches between positive and negative control inputs. The first control input drives the system to one of the two bold switch curves where the control input is switched and the states are led to the origin. The parabolic trajectory of the switch curves is given by the following equation:

$$x_1 = \zeta_1 - \frac{x_2^2}{6a_y} + \frac{\zeta_2^2}{6a_y} \tag{55}$$

where ζ_1 and ζ_2 represent the initial condition. The control trajectory in the α, β plane are 2x1 ellipses that become circles if plotted in the $x_3 = (n/4)\beta$, $x_4 = (1/4)\dot{\beta}$ plane as shown in Fig. 3.

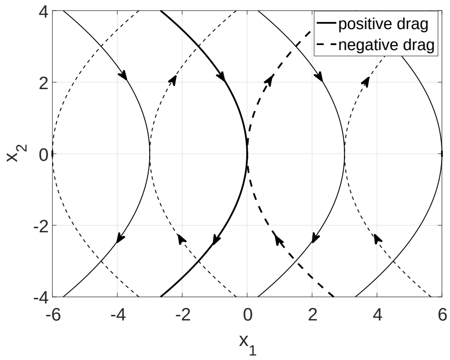

Figure 2: Control trajectories in the $\bar{y}, \dot{\bar{y}}$ plane

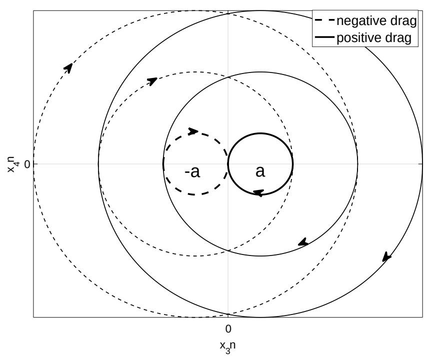

Figure 3: Control trajectories in the $\beta, \dot{\beta}$ plane

The switching strategy requires the evaluation of the switching curves based on the knowledge of the current position and velocity states and of the differential drag acceleration. In this work, the above guidance strategy is implemented using estimated values of the states and of the differential drag acceleration, as provided by the Relative Navigation module. The output of the Guidance is a decision to switch to one of the three possible modes of operation: positive, negative or zero differential drag. The decision is passed on to the Attitude Control module yielding the calculation of a desired attitude quaternion for each of the two satellites in formation.

6. Numerical Simulation

This section is concerned with the description of the satellites' dynamics simulator.

DOI: 10.13009/EUCASS2017-264

6.1 Physical model description

Five reference frames are used in this simulator. The Earth Centered Inertial (ECI), denoted by $\mathcal{I}$, two Local Vertical Local Horizontal (LVLH) frames centered at the Leader and Follower locations, denoted by $\mathcal{H}_L$ and $\mathcal{H}_F$, respectively, and two body frames centered at the satellites' centers of gravity, denoted by $\mathcal{L}$ and $\mathcal{F}$, respectively, or simply by $\mathcal{B}$ when the descriptions are identical for both satellites. The definitions of these frames and the computations of the Direction Cosine Matrices (DCM) follow standard textbooks descriptions (see for instance [14, 15]). In this work we adopt the following symbology: $D^{\mathcal{B}}_{\mathcal{A}}$ and $\mathbf{q}^{\mathcal{A}}_{\mathcal{B}}$ denote the DCM and the quaternion from frame $\mathcal{A}$ to frame $\mathcal{B}$. The dynamics of the orbital motion are simulated in the ECI frame. The satellite position and inertial velocity are denoted by $\mathbf{r}_I$ and $\mathbf{v}_I$, respectively. The acceleration due to the gravity field, denoted by $\mathbf{a}_G$, is computed using the Matlab function "gravitysphericalharmonic" that implements the mathematical representation of high orders spherical harmonic planetary gravity based on planetary gravitational potential. The solar radiation pressure and third-body accelerations due to the Sun and Moon are neglected. The drag acceleration, denoted by $\mathbf{a}_D$, is calculated based on a classical aerodynamics representation of the drag force, i.e., the pressure differential effects are lumped into a single force acting on the center of pressure of each satellite's panel. It is proportional to the dynamic pressure, the panel's cross-sectional area of reference normal to the flow, denoted by $S_i, i = 1, 2...$, and to the drag coefficient of the panel, C_{Di}. The satellites shapes are represented through their panels locations defined in the body frames. The centers of pressure are assumed to be coinciding with the geometric centers of the panels. The resulting drag force, denoted by $\mathbf{f}_D$, is calculated as the sum of the drag forces acting on the satellites' panels. The calculation of the panels' areas normal to the flow, $S_i, i = 1, 2, ...$, involves the calculation of the velocity vector relative to the atmosphere, denoted by $\mathbf{v}_a$. Calculation of $\mathbf{v}_a$ assumes an atmosphere co-rotating with the Earth at the nominal Earth rotation rate Ω_E. The calculation of the dynamic pressure requires the velocity and the atmospheric density, denoted by ρ, at the satellites' locations. The values of the atmospheric density are retrieved from a state-of-art semi-empirical model, namely the United States Naval Research Laboratory Mass Spectrometer and Incoherent Scatter Radar Exosphere (NRLMSISE-00 Atmosphere Model [5]). The calculation of the panels' areas normal to the flow are functions of the satellite's attitudes and the associated ballistic coefficients represent the indirect control variables in the proposed orbital motion guidance scheme. The satellites rotational motions around their centers of gravity are described by coupled kinematics and dynamics equations. The kinematics are expressed in terms of the attitude quaternion, denoted by $\mathbf{q}$, from the inertial frame $\mathcal{I}$ to the satellite's body frame. The angular velocities of the body frames are with respect to the inertial frame $\mathcal{I}$, resolved along the body frames, $\mathcal{L}$ and $\mathcal{F}$, and denoted by ω_L and ω_F, respectively. The Euler's equations describe the time evolution of ω for a given tensor of inertia, denoted by J, and external torques. These torques result from the sum of the command torques, $\mathbf{T}_c$, calculated in the Attitude Control module, and of the disturbance torques. The disturbance torques include a Drag torque, denoted by $\mathbf{T}_D$, and a Gravity-Gradient torque, denoted by $\mathbf{T}_{GG}$. The Drag torque is computed as the sum of the panels' drag torques evaluated using the panels drag forces and the panels arm vectors. Each panel's moment arm is a body fixed vector, denoted by ℓ_i, from the satellite center of gravity to the panel center of pressure. The gravity gradient torque, $\mathbf{T}_{GG}$, is calculated using a well known approximation model assuming a central and uniform gravity field.

6.2 Numerical simulator summary

The following equations summarize the simulation of each of the two satellites. The subscripts L and F are omitted for the sake of simplicity.

$$\dot{\mathbf{r}}_I = \mathbf{v}_I \tag{56}$$

$$\dot{\mathbf{v}}_I = \mathbf{a}_G + \mathbf{a}_D \tag{57}$$

$$\dot{\mathbf{q}} = \frac{1}{2}\begin{bmatrix} -[\omega\times] & \omega \\ -\omega & 0 \end{bmatrix}\mathbf{q} \tag{58}$$

$$\dot{\omega} = J^{-1}\left(J\,\omega\times\,\omega + \mathbf{T}_c + \mathbf{T}_D + \mathbf{T}_{GG}\right) \tag{59}$$

DOI: 10.13009/EUCASS2017-264

The Drag acceleration calculations are performed according to the following equations:

$$\mathbf{a}_D = \frac{1}{m}\mathbf{f}_D \tag{60}$$

$$\mathbf{f}_D = \sum_i \mathbf{f}_{Di} \tag{61}$$

$$\mathbf{f}_{Di} = \frac{1}{2}\rho C_{Di} S_i (\mathbf{v}_a^T D_{\mathcal{I}}^{\mathcal{B}} \mathbf{n}_i)(-\mathbf{v}_a)\ i = 1, 2... \tag{62}$$

$$\mathbf{v}_a = \mathbf{v}_I - \Omega_E \times \mathbf{r}_I \tag{63}$$

where the DCM matrix $D_{\mathcal{I}}^{\mathcal{B}}$ is readily computed using the inverse quaternion $\mathbf{q}^{-1}$. This factor clearly shows the coupling of the attitude and the orbital motions due to the drag force. Notice that the drag acceleration calculations mostly involve variables expressed in the inertial frame. Only the panels outward unit vectors, denoted by $\mathbf{n}_i$, are given in the body frames. The model accounts for potentially different areas and drag coefficients for each panel. The summation is done over the number of panels that actually “see” the air flow. For a cubic shape satellite that number is three at any time. The Drag torque calculations are performed as follows:

$$\mathbf{T}_{Di} = \ell_i \times \left(D_{\mathcal{B}}^{\mathcal{I}} \mathbf{f}_{Di}\right)\ i = 1, 2... \tag{64}$$

$$\mathbf{T}_D = \sum_i \mathbf{T}_{Di} \tag{65}$$

showing anew the coupling of the orbital and attitude motion. Notice that the torques are evaluated in the body frames, requiring the axes transformation from $\mathcal{I}$ to $\mathcal{B}$ of the individual drag forces. The Gravity-Gradient torque is expressed as follows [7, 15]:

$$\mathbf{T}_{GG} = 3\frac{\mu}{|\mathbf{r}_I|^3}\mathbf{a}_3 \times J\mathbf{a}_3 \tag{66}$$

where μ denotes the Earth gravitational constant and $\mathbf{a}_3$ denotes the Nadir unit vector from the satellite to the Earth center. That vector coincides with the negative unit vector in the X-direction of the $\mathcal{H}$ frame. The system of equations (56)-(66) summarizes the calculations performed in order to compute the true values of the inertial position, inertial velocity, quaternion, and angular velocity of each satellite. The relative navigation module however provides estimates of the relative position, denoted by $\mathbf{r}$, and of the relative velocity, $\dot{\mathbf{r}}$, of the Follower with respect to the Leader, resolved in the $\mathcal{H}_L$ frame. It also estimates the differential drag acceleration, denoted by $\mathbf{d}$ in Eq. (1) or a_y in Eq. (53), which is required in the estimate propagation stage of the Kalman filters and in the Guidance algorithm, respectively. The following equations describe how the true values of the relative position, relative velocity and of the differential drag, resolved along the frame $\mathcal{H}_L$, are obtained:

$$\mathbf{r}^o = D_{\mathcal{H}_L}^{\mathcal{I}}(\mathbf{r}_{I,F} - \mathbf{r}_{I,F}) \tag{67}$$

$$\dot{\mathbf{r}}^o = D_{\mathcal{H}_L}^{\mathcal{I}}[\mathbf{v}_{I,F} - \mathbf{v}_{I,L} + \omega_{\mathcal{H}_L} \times (\mathbf{r}_{I,F} - \mathbf{r}_{I,F})] \tag{68}$$

$$\mathbf{a}_{DD}^o = D_{\mathcal{H}_L}^{\mathcal{I}}(\mathbf{a}_{D,F} - \mathbf{a}_{D,L}) \tag{69}$$

where $\mathbf{r}_{I,L}$, $\mathbf{r}_{I,F}$, $\mathbf{v}_{I,L}$, $\mathbf{v}_{I,F}$ denote the inertial positions and velocities of the Leader and the Follower, respectively, and $\omega_{\mathcal{H}_L}$ denotes the angular velocity vector of the frame $\mathcal{H}_L$ with respect to the inertial frame resolved in $\mathcal{H}_L$.

7. Numerical Results

This section presents the performances of the proposed Guidance, Control and Navigation scheme obtained through numerical simulations. General parameters related to the orbits and to the satellites are shown in Table 1 and parameters used in the Relative Navigation Design Models are shown in Table 2. The simulations start with the two satellites on the same orbit and the Follower in front of the Leader by 70 km along the y-axis of the $\mathcal{H}_L$ frame.

7.1 Constant and known air density: Ideal guidance

The air density is assumed to be constant and known, equal to a typical nominal value at 400 km height, $\rho_0 = 5 \cdot 10^{-10}$ kg m^{-3}. Assuming that the satellites are instantaneously and perfectly achieving the desired relative attitude results in a constant and known differential drag acceleration, $a_y = 4.5 \cdot 10^{-4}$ m s^{-2}, which is either positive or negative according

DOI: 10.13009/EUCASS2017-264

Table 1: General parameters

Parameter	symbol	Value
Orbit altitude	h [km]	400
Nominal density	ρ_0 [kg m^{-3}]	$5 \cdot 10^{-10}$
Orbit eccentricity	e [-]	$5 \cdot 10^{-4}$
Orbit inclination	i [deg]	51.64
Principle moments of inertia	J_{ii} [kg m^2]	(0.0889,0.1162,1261)
Mass	[kg]	6.543
Nominal differential drag acceleration	a_y [m s^{-2}]	$4.5 \cdot 10^{-4}$
Max. magnetorquer dipole	m_{max} [Am^2]	0.1
Max. reaction wheel acceleration	$\dot{h}_{max}$ [Nm]	$1 \cdot 10^{-5}$
Max. reaction wheel angular momentum	h_{max} [Nms]	$1 \cdot 10^{-3}$

Table 2: Filter parameters

Parameter	Value
gyroscopes sampling time [sec]	2
vector measurements sampling time [sec]	60
σ_b [arcsec]	100
σ_u [-]	$2 \cdot 10^{-4}$
σ_v [deg s^{-1}]	$1 \cdot 10^{-5}$
$\hat{\mathbf{q}}_0$ [-]	(0,0,0,1)
$\hat{\mu}_0$ [deg s^{-1}]	(0,0,0)
$P_A(0)$ (Model 0, Model 1)	diag(0.1 I_3, 0.001 I_3)
relative position sampling time [sec]	60
σ_N [m]	1
$\hat{\mathbf{x}}_0$ [m]	(0,0,0,0,0,0)
$P_N(0)$ (Model 0, Model 1)	100 I_6

to the relative satellites orientations. This enables checking the performances of the ideal guidance algorithm from Ref. [3]. Figures 4 to 7 describe the maneuvers of the ideal guidance algorithm. Along each trajectory curves are drawn 'quarter of orbits'-ticks that time the maneuvers. Figure 4 shows the trajectory in the mean motion plane. At the first switch point the Follower flips to a minimum drag attitude and the Follower to a maximum drag attitude - as shown by the symbols '-|' near the switch point. The Leader slides below the Follower and takes speed. At approximately 1.3 orbit, while the Follower travels about 5 km above and 35km in front of the Leader, the trajectory in the mean motion plane hits the switching curve triggering a flip in the satellites' attitudes to the opposite differential drag mode. Then the trajectory slides along the switching curve until the end of guidance level 1 when the mean position hits the origin in Fig. 4 around 2.7 orbit. At that point the Follower again adopts a drag lean attitude and the guidance levels 2 and 3 start. These are concerned with the control of the deviations around the mean position and are described in Figures 6,7. They involve a series of switches among the three possible modes, positive, negative, and zero differential drag, until the origin is reached within 7.5 orbits. Notice that these maneuvers imply that the mean position itself is set to motion, leaving and returning eventually to the origin, via sequence of so-called "hat-shape" maneuvers, referring to the shape of the trajectories in the mean motion plane. The relative motion in the $\mathcal{H}_L$ frame can be captured in Fig. 5: it shows that most of the maneuver is performed during level 1 guidance with a distance closing from 70 km, while the level 2 and 3 guidance induces deviations of about10 km along track and 2 km in the radial direction before converging to the origin. This hints at the fact that level 1 guidance will be likely most relevant in 'real-life' scenarios while level 2 and 3 guidances will be 'nice to have', if possible. This 'blue sky' validation check provides a 10 m accuracy in the guidance performances within 8 orbits.

DOI: 10.13009/EUCASS2017-264

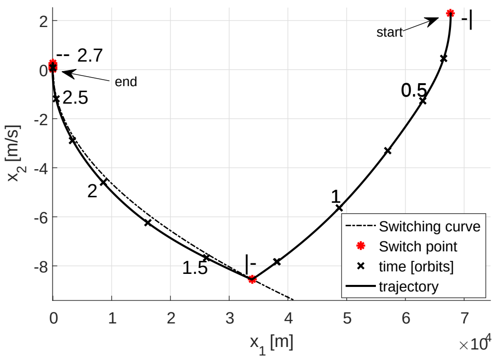

Figure 4: Constant air density: trajectory in the mean motion plane - guidance level 1

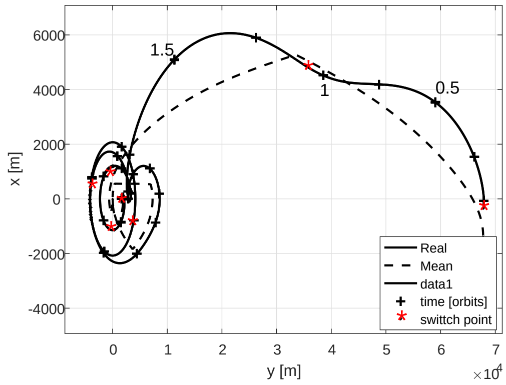

Figure 5: Constant air density: relative motion in $\mathcal{E}_L$

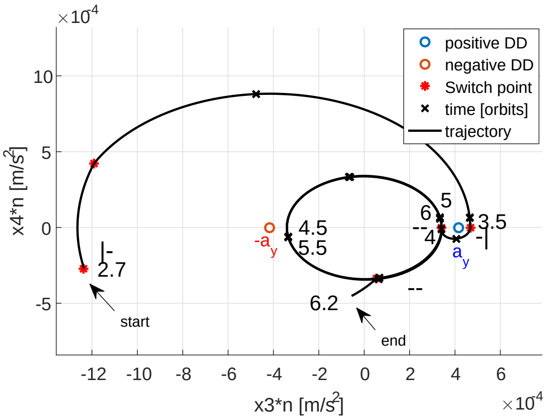

Figure 6: Trajectory in the deviations motion plane - guidance level 2

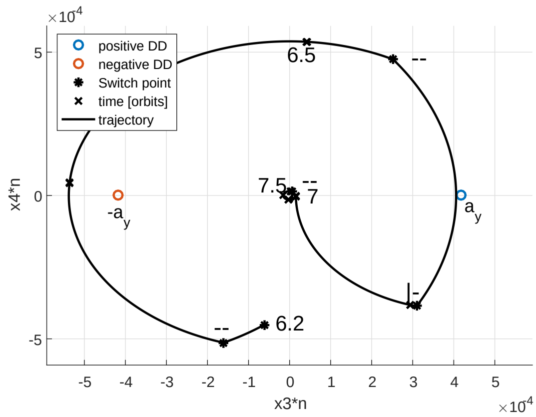

Figure 7: Trajectory in the deviations motion plane - guidance level 3

7.2 Time-varying air density - high solar activity

7.2.1 Guidance performances with full information

The air density is assumed to vary according to the plot in Fig. 8-top, showing very high deviations from the nominal density value previously assumed. Full information and perfect attitude control actuation are assumed, hence the differential drag is known, as depicted in Fig. 8-bottom. The time-varying differential drag induces a time-varying switching curve which creates the sluggish trajectory of the mean relative position (dotted line in Fig. 9). Further the high variability of the density is responsible for the bulbs in the actual relative trajectory in the $\mathcal{H}_L$ (plain line in Fig. 9). Application of the level 1 guidance scheme with a high-variability realistic density yields a serious degradation in performances: 2 km in the radial direction and 10 km in the in-track direction at 2.7 orbit in the maneuver. This emphasizes the criticality of the time invariance of the differential drag in the guidance algorithm.

7.2.2 Attitude Control and Determination performances

Attitude control is implemented in order to relax the unrealistic assumption of perfect and instantaneous attitude 'flips'. Attitude estimates have two impacts: 1/ they contribute to the differential drag estimation, which is used in the relative navigation calculations; the differential drag is also used in the switching curves construction and thus impacts the guidance performances, 2/ they contribute to the attitude tracking errors and thus impact the attitude control performances. The attitude control gains were chosen by trial and errors such as to yield a settling time of approximately 5 mn and

DOI: 10.13009/EUCASS2017-264

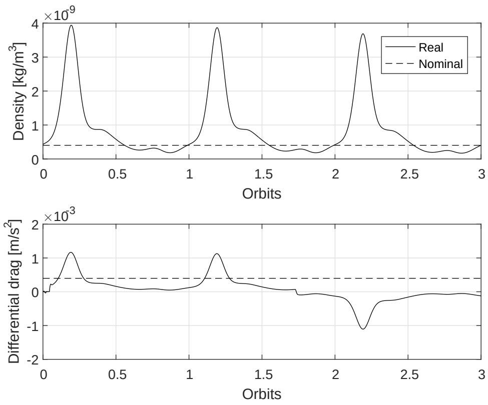

Figure 8: High solar activity: air density and DD acceleration

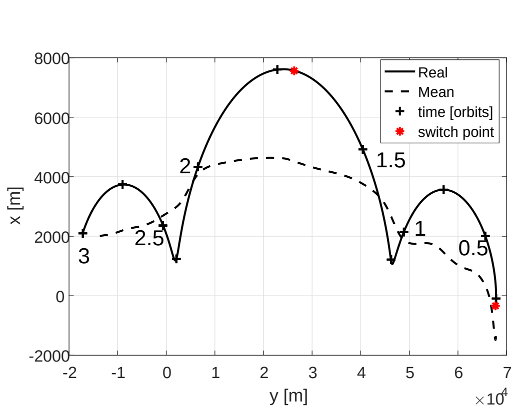

Figure 9: High solar activity: Relative motion in $\mathcal{E}_L$ with full information level 1 guidance

a steady state error in tracking of less than 3 degrees. Figures 10, 11 summarize the attitude control performances. Figure 11 depicts the time history of the attitude pointing error, which settles about 2.3 degrees after each switch point. Figure 11 shows the drag and control torques on both the Leader and Follower. It pictures the relatively high torques along the z-body axes required for the 90 degrees maneuvers within 5mn. It shows the relatively high value of the drag torque along the other axes which is the dominant perturbations that the control torques must counteract continuously.

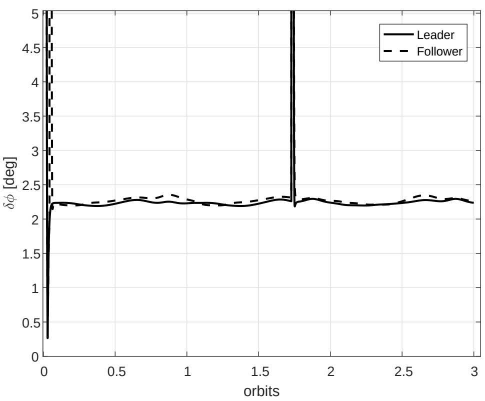

Figure 10: High solar activity: Angular pointing error

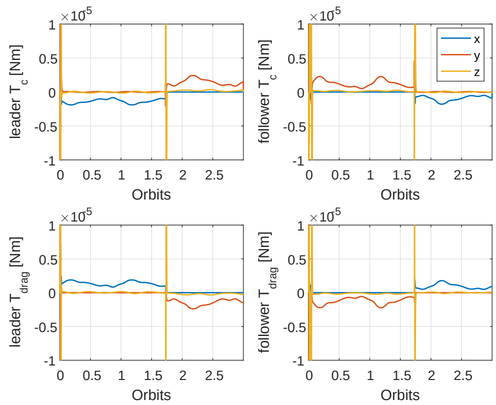

Figure 11: High solar Activity: drag and control torques in Leader and Follower

7.2.3 Navigation performances

Figures 12,13 summarize the performances of the navigation filters for the various design models. The 'Model 0' plots refer to the Kalman filter where the actual time-varying air density is exactly known. The 'Model 1' plots refer to the Kalman filter that treats the density as a constant ρ_0 corrupted by white noise. The 'Model 2' plots corresponds to the Kalman filter that estimates the variable part of the density, along with the relative motion. The 'Model 3' plots refer to the robust H_∞ filter estimates the relative motion under a bi-topic uncertainty on the density. Several facts can be noticed from the figures: 1/ the robust H_∞ filter is the quickest to converge, 2/ the robust H_∞ filter is the least sensitive to the high variability in the real air density, 3/ all filters converge in steady state to relatively good accuracies, 5 m in radial direction, 10 m along track, and 5 cm/s in velocities. It can be further noticed that the Model 0 Kalman filter shows the best accuracy in steady-state, as expected, that the Model 2 filter is the most sensitive to the high variability in

DOI: 10.13009/EUCASS2017-264

the density, and that the robust $H\infty$ filter is noisier than the Kalman filters in steady state. The navigation performances are better (by orders of magnitudes) than the guidance performances, as they should. The best filter candidate for the high solar activity case appears to be the robust H_∞ filter since it allies quicker convergence, lower sensitivity to high variations in the density, and a similar steady-state accuracy to the Model 1 filter.

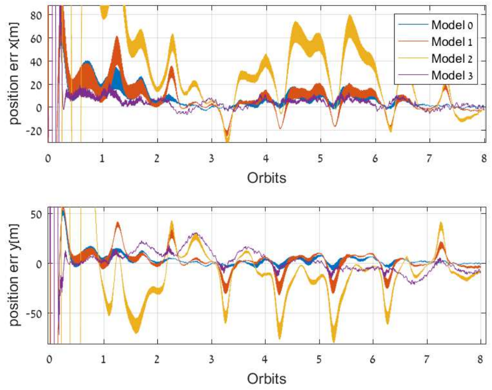

Figure 12: High solar activity: position estimation errors

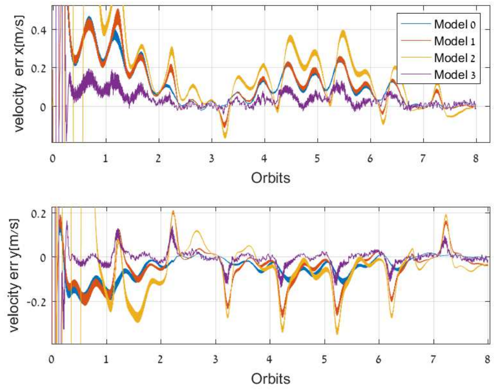

Figure 13: High solar activity: velocity estimation errors

7.2.4 Guidance performances with Attitude Control and Navigation

Figures 14,15 summarize the performances of the proposed guidance, navigation and control scheme in the case of high variability density. Figure 14 depicts the estimated and true trajectories in the mean motion plane. The estimated trajectory stems from the H_∞ filter. The navigation errors appear small compared to the actual distances to travel. The first switch point takes place at 2.2 orbit, much later than the nominal 1.7 orbit of the ideal guidance law. The remainder of the curve is far from following the switching curve. An additional switch is taking place around 6.6 orbits. Figre 15 shows the relative trajectory in the $\mathcal{H}_L$.The mean position and the true position reach a neighbourhood of the origin within 8 orbits, yielding guidance accuracies of about 2 km in both the radial and the in-track directions.

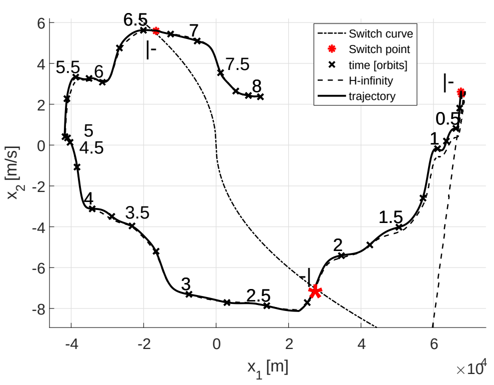

Figure 14: High solar activity: trajectory in the mean motion plane - guidance level 1

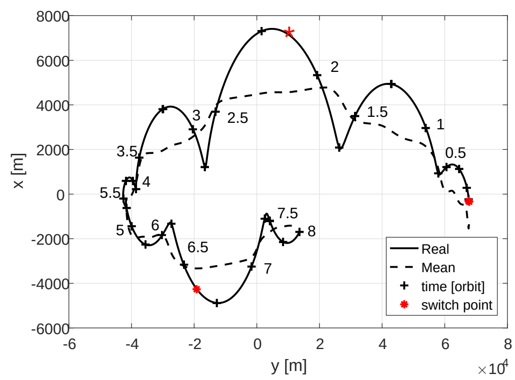

Figure 15: High solar activity: relative motion in $\mathcal{E}_L$ - guidance level 1

DOI: 10.13009/EUCASS2017-264

8. Conclusion

This work is concerned with the development of algorithms for guidance, navigation and control, including attitude determination and control, for formation flying of small satellites via differential drag only along low Earth orbits. A baseline guidance scheme presented in the literature was chosen, where the differential was assumed fully controllable, piece-wise constant, and known. Several 'real-life' features were added: a high variability air density, an attitude control algorithm that enables maneuvers to modify the ballistic coefficient, an attitude determination algorithm processing typical vector measurements available for small satellites, and several relative navigation filters based on various air density information modeling. The dynamics environment included high-order gravity modeling for the orbit, drag and gravity-gradient torques as perturbations for the rotation. The ideal guidance scheme was tested on a two satellites formation flying on the orbit of the International Space Station starting with a range of 70 km. It enables closure of the distance down to 10 m within eight orbits. The 'real life' GNC/ADCS algorithms tested under the same conditions produced a final distance of about 2 km within eight orbits. The degradation in the performances is due to the high variability of an unknown air density, the relative navigation errors, and the attitude control errors, in order of dominance. The best relative navigation filter appears to be a robust H_∞ filter. A comparison of that filter with the various Kalman filters shows a quicker convergence, a lesser sensitivity to the jumps in the air density, a similar steady-state accuracy, albeit with a noisier behavior.

References

[1] T. D. Maclay and Christopher Tuttle. Satellite stationkeeping of the orbcomm constellation via active control of atmospheric drag: Operations, constraints, and performance (aas 05-152). *Advances in the Astronautical Sciences*, 120(1):763, 2005.

[2] C.L. Leonard. *Formationkeeping of spacecraft via differential drag*. PhD thesis, 1986.

[3] C. L. Leonard, W. M. Hollister, and E. V. Bergmann. Orbital formationkeeping with differential drag. *Journal of Guidance, Control, and Dynamics*, Vol. 12:108–113, 1989.

[4] T. Reid and A. K. Misra. Formation flight of satellites in the presence of atmospheric drag. *Journal of Aerospace Engineering*, 3(1):64, 2011.

[5] J.M. Picone et al. Nrlmsise-00 empirical model of the atmosphere: Statistical comparisons and scientific issues. *Journal of Geophysical Research: Space Physics*, 107(A12), 2002.

[6] J. R. Wertz. *Spacecraft attitude determination and control*, volume 73. Springer Science & Business Media, 2012.

[7] J. L. Crassidis and F. L. Markley. *Fundamentals of Spacecraft Attitude Determination and Control*. Springer, New York, 2014.

[8] J. Reijneveld and D. Choukroun. Attitude control of the delfi-n3xt satellite. In *AIAA-2011-6434, AIAA Guidance, Navigation, and Control Conference*, 2011.

[9] H. Weiss B. Wie and A. Arapostathis. Quaternion feedback regulators for spacecraft eigenaxis rotation. *AIAA - Journal of Guidance, Control and Dynamics*, 1989.

[10] A. Shiryaev M. Guelman, R. Waller and M. Psiaki. Testing of magnetic controllers for satellite stabilization. *Acta Astronautica*, 56:231–239, 2005.

[11] R. Mortensen. A globally stable linear attitude regulator. *Int. Journal of Control*, 8:297–302, 1968.

[12] J. R. Forbes and C. J. Damaren. A geometric approach to spacecraft attitude control using magnetic and mechanical actuation. *Journal of Guidance, Control, and Dynamics*, Vol. 33, 2010.

[13] W. H. Clohessy and R. S. Wiltshire. Terminal guidance system for satellite rendezvous. *Journal of the Aerospace Sciences*, Vol. 27:653–658, 1960.

[14] D. A. Vallado. *Fundamentals of Astrodynamics and Applications*. Space Technology Library, 2 edition, 2001.

[15] B. Wie. *Space vehicle dynamics and control*. AIAA, 1998.